Near-Zero Volume Expansion Nanoporous Silicon as Anode for Li-ion Batteries

Journal of The Electrochemical Society, 2022 **169** 080506

Near-Zero Volume Expansion Nanoporous Silicon as Anode for Li-ion Batteries

Fabio Maroni,[1] Marco Spreafico,[2] Axel Schönecker,[2] Margret Wohlfahrt-Mehrens,[1] and Mario Marinaro[1,z]

[1]*Zentrum Für Sonnenenergie Und Wasserstoff Forschung Baden-Württemberg (ZSW), Helmholtzstraße 8, 89081, Ulm., Germany*
[2]*E-magyB.V., Bijlestaal 54a, 1721 PW Broek op Langedijk, The Netherlands*

In this work, novel near-zero volume expanding Si-dominant electrodes are presented as promising anodes for next-generation Li-ion batteries. The electrodes contain micrometer-size nano-porous Silicon particles with a carefully tuned morphology and synthesized via a scalable and cost-effective route. Volume expansion during electrochemical Li-Si alloying/de-alloying is found to be almost completely suppressed. Bi-layer pouch cells manufactured with the abovementioned Si-anodes, having industrial relevant areal capacities (⩾3 mAh cm^{-2}), and $LiNi_{0.6}Mn_{0.2}Co_{0.2}O_2$ cathodes, show indeed negligible volume expansion as demonstrated by *operando* dilatometric measurements during galvanostatic cycling and *post-mortem* SEM cross-sectional analysis.
 [DOI: 10.1149/1945-7111/ac8628]

Manuscript submitted June 3, 2022; revised manuscript received July 20, 2022. Published August 8, 2022.

Supplementary material for this article is available online

Current generation of Li-ion batteries (LIBs) rely on the extensively studied and industrially robust graphite anode.[1] Up to now, even in high-end LIBs only few weight% of Si or SiO_x is used to increase the energy. Increasing the Si content in the anode, together with the development of high-capacity cathode materials, are two of the main routes available to further push the boundaries in term of specific energy and energy density at the material level. This is the state-of-the-art to be overcome, in terms of practical areal capacities, cycling life and stability.[2] Despite the desirable features of Si, such as a low operating potential, abundancy and a very high theoretical specific capacity of 3579 mAh g^{-1} at room temperature,[3] the development of Si-dominant anodes remains still a challenge. As it is well known, the practical implementation of Si-dominant anodes in commercial LIBs is hindered by the considerable volume expansion during the Li-Si (de)alloying processes, which eventually leads to particle pulverization cracking[4] and electrode delamination,[5] in turn leading to short cycle life and safety concerns. Few examples of evaluation of the silicon expansion studied in pouch or cylindrical cells can be found in literature.[6–9] Reducing particle size to a nanoscale level[10] in order to mitigate these issues might not be the best option, particularly when considering handling, costs and electrode manufacturing related issues. Therefore, a careful and cost-effective tuning of particle morphology of micrometer-sized-Si is essential to maximize cell performance and at same time keep costs at an acceptable level, in a way that Si price per kWh is comparable to that of graphite. In this work, a novel micrometer-sized nano-porous Si material, is presented and used to prepare anodes with industrially relevant areal capacities. Si-dominant anodes have been developed with a tuned formulation using poly-Acrylic Acid as polymeric binder. The Si electrodes electrochemical performance have been evaluated in both half- (coin-type) and full-cell configurations (bi-layer soft pouches). Test results demonstrate a near-zero volumetric expansion during *operando* electrochemical dilatometry experiments.

Experimental

The E-magy silicon material (E-magy 35–400 D2) was morphologically characterized by means of SEM microscopy. This silicon material is produced by a rapid directional solidification process with $35\%_{vol.}$ internal porosity. The crystallized material is milled to a powder with a D50 value of 2 μm. NMC 622 (BASF®) cathodes for full cell tests were prepared on an industrial pilot line (LACOM©). Aqueous Si-electrode slurries were prepared in 80:10:5:5 ratio between the active material, PolyAcrylic Acid (PAA) binder (Aldrich® M_w = 250 k kg mol^{-1}), KS6L graphite and superC45 (Imerys®) conductive additive, respectively. PAA Binder has been used without neutralization. Slurries were cast on a 12 μm Cu current collector and dried at room temperature. Active material loading resulted to be of ~2.6 mg cm^{-2}– ~3 mg cm^{-2}. Electrodes were used as prepared without further calendering. Electrode porosity has been estimated at ~64%. Of note that the porosity of the Si material itself is of ~35%. Half-cells were assembled in an Ar-filled glovebox (Mbraun®) with a 450 μm Li counter electrode (MTI), using a GF/A glass fiber separator. The bi-layer pouch cells were manufactured in a dry-room with a dew point of −65 °C, using a 150 μm laminated coffee-bag and a Celgard 2325 separator. The electrolyte is $LiPF_6$ 1M in EC:EMC 3:7 + 10% FEC for all electrochemical tests, 150 μl for the CR2032 cells and 1.5 ml for the bi-layer pouch format. Electrochemical tests were carried out on a BasyTec (BasyTec GmbH) test system in CR2032 cell format for half-cell experiments in the $0.005 < U(V) < 1.000$ voltage range, while full cells were cycled in the $2.500 < U(V) < 4.120$ voltage range. All pouch cells were pressurized to 0.35 MPa and Keyence GT2 sensors were applied to in-house made cell holders for *operando* dilatometry measurements.[11–13]

Results and Discussion

Figure 1 depicts the morphology of the as synthesized micrometer-sized nano-porous material, as investigated by Scanning Electrode Microscopy (SEM).

As can be seen in Figs. 1b and 1c, the Si material shows a morphology made of micrometer-sized Si particles, which are characterized by a high number of nano-pores. The open pores, which run through the depth of the silicon from front to back, contribute to an improved volume expansion buffering during extended electrochemical cycling. From BET measurements, silicon has a specific surface of 12.99 m^2 g^{-1} and an average pore size diameter of ~400 nm.

Figures 2a–2c summarizes the obtained electrochemical results. In Fig. 2a, a half-cell test in CR2032 format is reported. Electrode slurry formulation has been optimized in lab-scale in terms of binder[14] (PAA), conductive additive (SuperC45 and KS6L graphite) and solid content to obtain reliable performance, resulting in very

[z]E-mail: mario.marinaro@zsw-bw.de

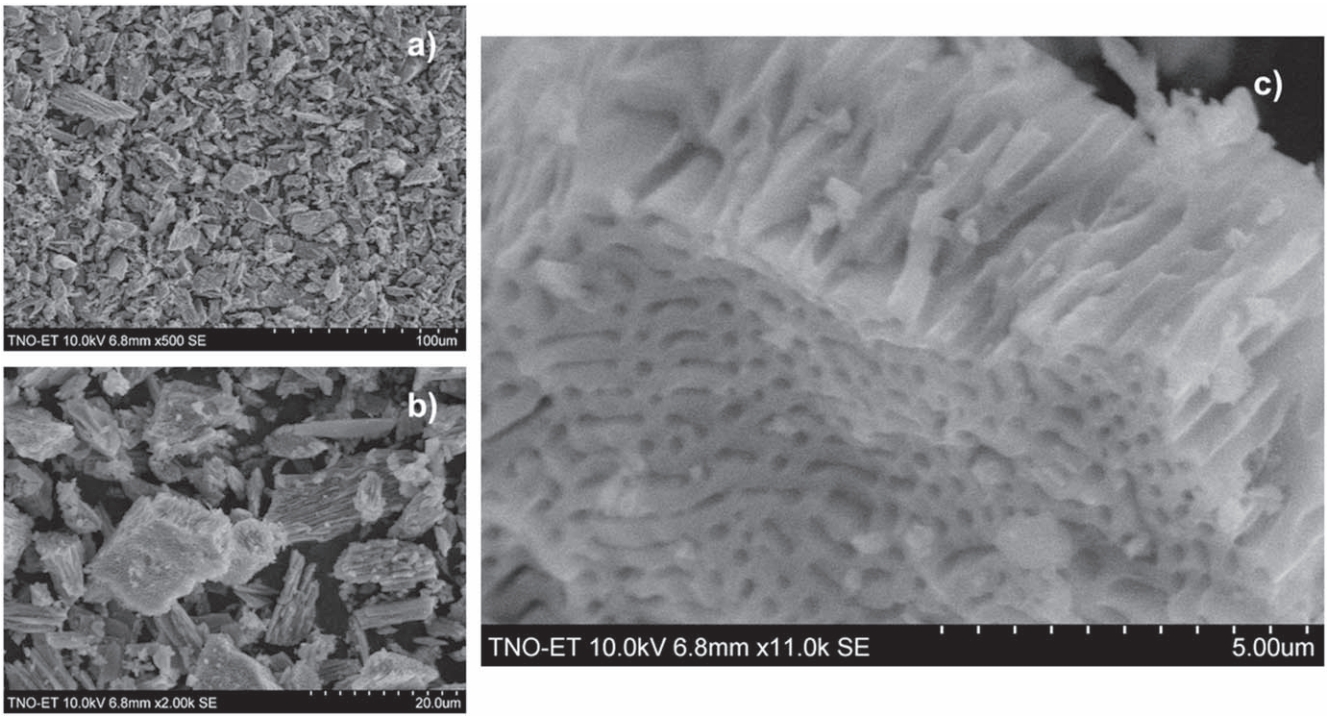

Figure 1. SEM micrographs of the E-magy Si material at different magnifications: (a) 500×, (b) 2000× and (c) 11000×.

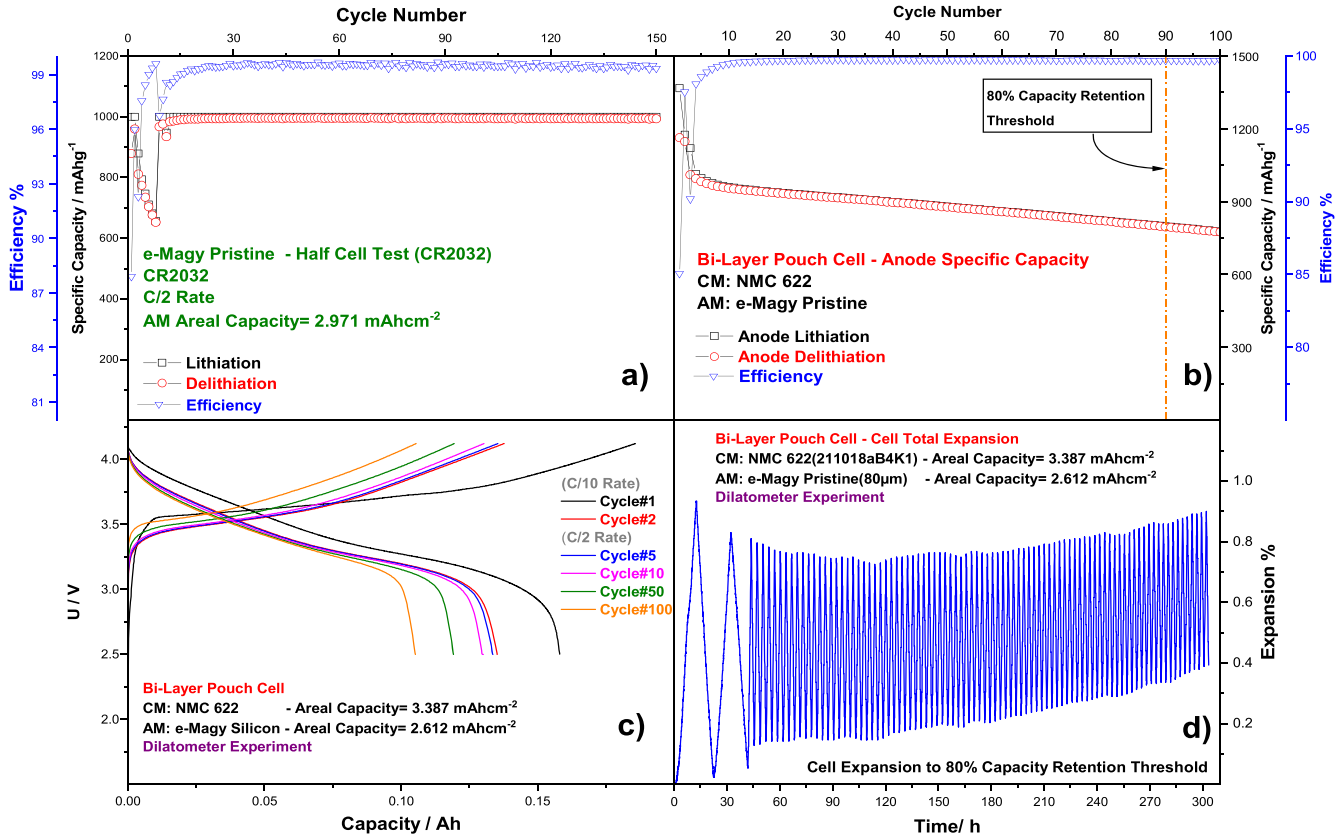

Figure 2. EM-01 Electrochemical Characterization (a) Half-Cell Test at C/2 Rate, (b) Bi-Layer pouch cell experiment at C/2 rate, (c) Pouch-cell charge/discharge profiles and (d) *operando* dilatometry experiment.

homogenous coatings within the interval of active material loading specified in the experimental part. To note that the anode specific capacity has been limited to 1000 mAh g^{-1} in half-cells, resulting in electrodes with areal capacities of ∼3 mAh cm^{-2}. Figure 2a shows the long-term cycling stability test of the Si-dominant electrodes, carried out at a C/2 rate (500 mA g^{-1} – 1.5 mA cm^{-2}), after two formation cycles at C/10, in the voltage window $0.005 < U(V) < 1.000$. The first cycle Irreversible Capacity Loss (ICL) for the

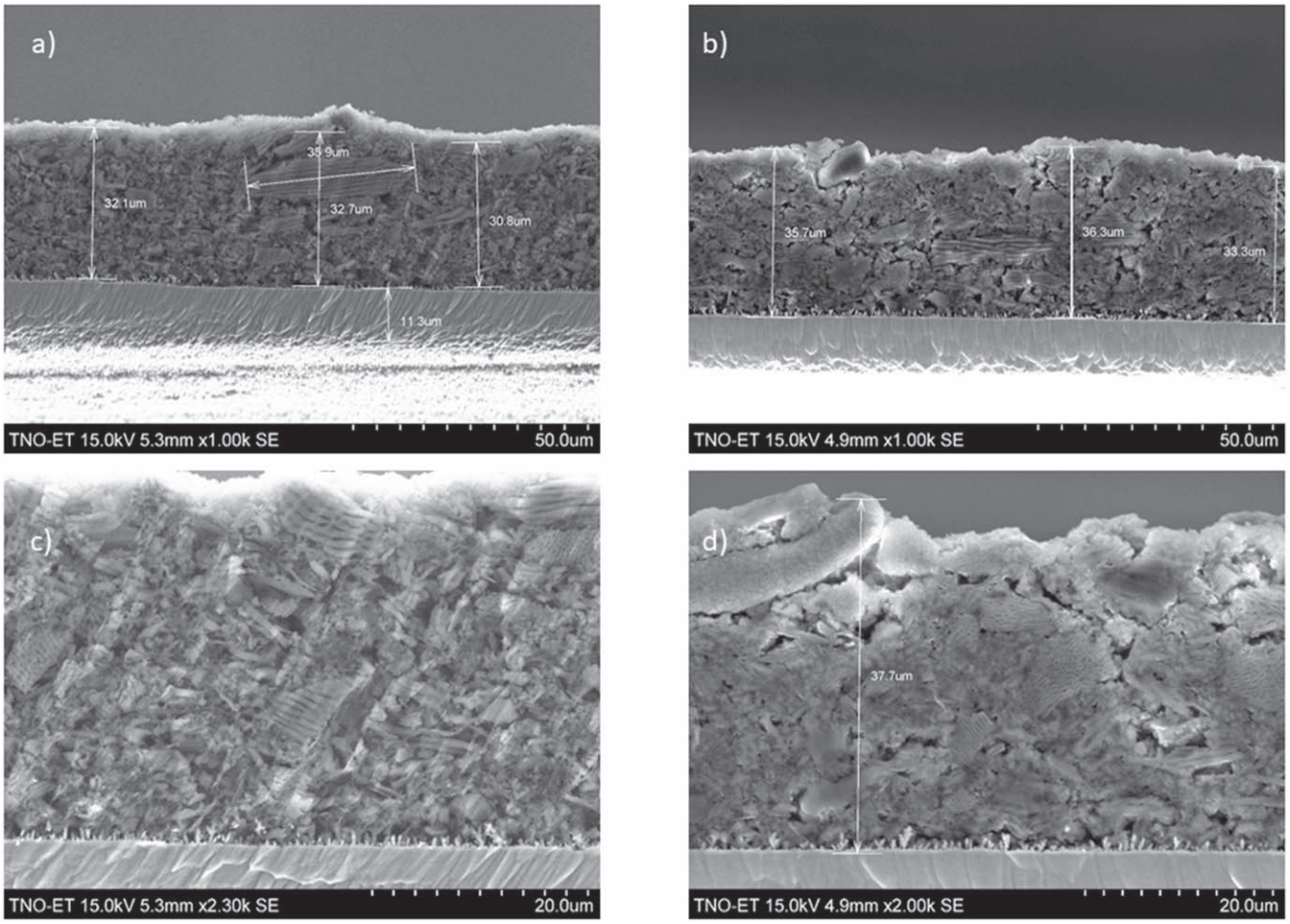

Figure 3. Electrode cross-sectional analysis recorded at various magnifications: (a) (c) pristine electrode and (b) (d) cycled electrode (200 galvanostatic cycles).

silicon material is of ∼12%, (121 mAh g^{-1}), which is a relatively low value.[15] As it can be seen, the electrode material is generally stable up to cycle 150, with a constant (dis)charge capacity of 1000 mAh g^{-1} and an average coulombic efficiency of 99.40%. Only during the first cycles following the slow formation at C/10, a quick, but temporary, decrease in the specific capacity is evidenced, before reaching the 1000 mAh g^{-1} target. This has been assigned to a progressive material activation within the first few cycles, which has been reported in literature.[16] Figure S1 (available online at stacks.iop.org/JES/169/080506/mmedia) shows selected galvanostatic profiles of the half-cell test. The first cycle reduction is characterized by a single long plateau due to the amorphization of Si upon lithiation.[17] Following cycles are characterized by a long sloping plateau from U = 0.500 V to U = 0.100 V and a second, shorter plateau, at voltages from U = 0.009 V to U = 0.060 V, in an increasing trend with cycle number.

In order to increase the energy in a battery cell, not only the reversible but also the irreversible capacity loss at the first cycle plays a very important role. We often therefore compare different anode materials on the basis of their efficient capacity, defined as it follows:

$$C_{eff} = \frac{C_e * C_p}{(C_p + C_i)}$$

in which, C_e is the reversible capacity of the anode, C_i is the anode irreversible capacity and C_p is the cathode reversible capacity. For the silicon material here presented, this value results to be of 584 mAh g^{-1}, which results to be more than doubled than state-of-the art graphite of 267 mAh g^{-1} (Check Table SI).[18,19,20]

In Fig. 2b, the electrochemical performance of a bi-layer pouch cell is showed. The cell was cycled following a similar protocol as the half-cell, with C/10 formation cycles and C/2 cycling rate in the 2.500 < U(V) < 4.120 cell voltage window. The cell had a first-cycle high coulombic efficiency of 85% and hit the 80% capacity retention threshold at cycle 90, with an average coulombic efficiency of 99.66%, which, considering the silicon dominant composition of the anode, combined with a 2.612 mAh cm^{-2} anode areal capacity (2.612 mg cm^{-2} Si mass loading), is a notable result. Figure 2c depicts the capacity profiles of selected cycles of the bi-layer pouch cell, showing a quite regular cycling during the charge step, while it is apparent that the cell discharge (anode dealloying) is the limiting step in the cell cycle life. Figure 2d shows cell response to repeated cycling during the *operando* dilatometry experiment. In the Expansion% vs time plot (Fig. 2d), periodical expansion/contraction of the cell can be clearly seen. Then, considering the cycling time required to reach the 80% capacity retention threshold, the cell expanded in total less than 1% of its original thickness. The corresponding thickness vs time plot of the nanoporous-Si anode is reported as Fig. S2 in the supporting information.

Figure 3 shows a cross-sectional analysis of pristine and cycled (*post-mortem)* Si electrode, after 200 galvanostatic cycles. On the one hand, electrode structure of the pristine electrode is characterized by a quite wide particle size distribution, and a porous structure. Morphology of primary particles is clearly visible and does not show signs of degradation due to slurry processing with respect to the

pristine powder (Figs. 1a–1c). On the other hand, while the cycled electrode retains a good packing and the original morphology is still visible, a certain number of cracks is introduced although no relevant expansion or delamination is revealed in accordance with the dilatometry results (Fig. 2). The ability of containing volume expansion on a macroscopic cell level could be explained by the nano-porous morphology and the specific capacity limitation, applied at a material level, used in these cycling tests. Literature data has confirmed the ability of nanowire morphology to contain volume expansion during (de)alloying processes.[21] Then, the available space in the long, longitudinally developed pores, can be seen as effective in avoiding particle cracking and degradation over extended cycling of pouch cells with industrially relevant areal capacities.

Conclusions

In conclusion, the presented nano-porous-Si material shows very promising and robust performance in a bi-layer pouch cell configuration, with industry relevant areal capacities of $\sim$3 mAh cm^{-2}. A porous and unique fused nanowire-like particle morphology acts as effective buffer towards volume expansion and this behavior has been confirmed by the electrochemical dilatometry experiments, which indicated only minimal volume expansion. Cross-sectional analysis comparison of pristine and cycled electrodes further confirmed the foundlings, showing that material morphology is retained during electrochemical cycling and despite the introduction of a limited number of cracks, electrode structure is maintained.

Acknowledgments

This research was partially supported by the Netherlands Enterprise Agency in the Innovation Credit Scheme under contract No. IK20044. The authors gratefully acknowledge the support from Dr. Peter Kalisvaart and Akam Osmanpour for SEM cross-sectional analysis and discussion.

ORCID

Fabio Maroni https://orcid.org/0000-0002-2534-5668
Mario Marinaro https://orcid.org/0000-0002-5954-0357

References

1. M. Armand et al., *J. Power Sources*, **479**, 228708 (2020).
2. M. Marinaro, D. Bresser, E. Beyer, P. Faguy, K. Hosoi, H. Li, J. Sakovica, K. Amine, M. Wohlfahrt-Mehrens, and S. Passerini, *J. Power Sources*, **459**, 228073 (2020).
3. M. N. Obrovac and V. L. Chevrier, *Chem. Rev.*, **114**, 11444 (2014).
4. M. N. Obrovac, *Current Opinion in Electrochemistry*, **9**, 8 (2018).
5. V. Vanpeene, J. Villanova, A. King, B. Lestriez, E. Maire, and L. Roué, *Adv. Energy Mater.*, **9**, 1803947 (2019).
6. G. Berckmans, L. de Sutter, M. Marinaro, J. Smekens, J. Jaguemont, M. Wohlfahrt-Mehrens, J. van Mierlo, and N. Omar, *Electrochim. Acta*, **306**, 387 (2019).
7. L. de Sutter, G. Berckmans, M. Marinaro, J. Smekens, Y. Firouz, M. Wohlfahrt-Mehrens, J. van Mierlo, and N. Omar, *Energies*, **11**, 2948 (2018).
8. L. de Sutter, G. Berckmans, M. Marinaro, M. Wohlfahrt-Mehrens, M. Berecibar, and J. van Mierlo, *J. Power Sources*, **451**, 227774 (2020).
9. D. Vidal et al., *J. Power Sources*, **514**, 230552 (2021).
10. X. H. Liu, L. Zhong, S. Huang, S. X. Mao, T. Zhu, and J. Y. Huang, *ACS nano*, **6**, 1522 (2012).
11. V. Müller, R. Bernhard, J. Wegener, J. Pfeiffer, S. Rössler, R.-G. Scurtu, M. Memm, M. A. Danzer, and M. Wohlfahrt-Mehrens, *Energy Technol.*, **8**, 2000217 (2020).
12. V. Müller, R.-G. Scurtu, M. Memm, M. A. Danzer, and M. Wohlfahrt-Mehrens, *J. Power Sources*, **440**, 227148 (2019).
13. V. Müller, R.-G. Scurtu, K. Richter, T. Waldmann, M. Memm, M. A. Danzer, and M. Wohlfahrt-Mehrens, *J. Electrochem. Soc.*, **166**, A3796 (2019).
14. R. Kasinathan, M. Marinaro, P. Axmann, and M. Wohlfahrt-Mehrens, *Energy Technol.*, **6**, 2256 (2018).
15. J. Hou, S. Qu, M. Yang, and J. Zhang, *J. Power Sources*, **450**, 227697 (2020).
16. M. Saito, K. Kato, S. Ishii, K. Yoshii, M. Shikano, H. Sakaebe, H. Kiuchi, T. Fukunaga, and E. Matsubara, *J. Electrochem. Soc.*, **166**, A5174 (2019).
17. M. N. Obrovac and L. J. Krause, *J. Electrochem. Soc.*, **154**, A103 (2007).
18. F. Jeschull, D. Brandell, M. Wohlfahrt-Mehrens, and M. Memm, *Energy Technol.*, **5**, 2108 (2017).
19. M. Marinaro, M. Weinberger, and M. Wohlfahrt-Mehrens, *Electrochim. Acta*, **206**, 99 (2016).
20. M. Marinaro et al., *J. Power Sources*, **357**, 188 (2017).
21. C. K. Chan, H. Peng, G. Liu, K. McIlwrath, X. F. Zhang, R. A. Huggins, and Y. Cui, *Nat. Nanotechnol.*, **3**, 31 (2008).